


Article

Isoniazid Linked to Sulfonate Esters via Hydrazone Functionality: Design, Synthesis, and Evaluation of Antitubercular Activity

Ebru Koçak Aslan ¹, Muhammed İhsan Han ², Vagolu Siva Krishna ³, Rasoul Tamhaev ^{4,5}, Cagatay Dengiz ⁶, Şengül Dilem Doğan ⁷, Christian Lherbet ⁴, Lionel Mourey ⁵, Tone Tønjum ^{3,8} and Miyase Gözde Gündüz ^{1,*}

¹ Department of Pharmaceutical Chemistry, Faculty of Pharmacy, Hacettepe University, Sıhhiye, Ankara 06100, Turkey

² Department of Pharmaceutical Chemistry, Faculty of Pharmacy, Erciyes University, Kayseri 38039, Turkey

³ Unit for Genome Dynamics, Department of Microbiology, University of Oslo, 0316 Oslo, Norway

⁴ LSPCMIB, UMR-CNRS 5068, Université Paul Sabatier-Toulouse III, 118 Route de Narbonne, CEDEX 9, 31062 Toulouse, France

⁵ Institut de Pharmacologie et de Biologie Structurale, Université Toulouse III—Paul Sabatier, Centre National de la Recherche Scientifique, 31077 Toulouse, France

⁶ Department of Chemistry, Middle East Technical University, Ankara 06800, Turkey

⁷ Department of Basic Sciences, Faculty of Pharmacy, Erciyes University, Kayseri 38039, Turkey

⁸ Unit for Genome Dynamics, Department of Microbiology, Oslo University Hospital, 0424 Oslo, Norway

* Correspondence: miyasegunduz@yahoo.com



Citation: Koçak Aslan, E.; Han, M.İ.; Krishna, V.S.; Tamhaev, R.; Dengiz, C.; Doğan, Ş.D.; Lherbet, C.; Mourey, L.; Tønjum, T.; Gündüz, M.G. Isoniazid Linked to Sulfonate Esters via Hydrazone Functionality: Design, Synthesis, and Evaluation of Antitubercular Activity.

Pharmaceuticals **2022**, *15*, 1301.

<https://doi.org/10.3390/ph15101301>

ph15101301

Academic Editors: Maria Matilde Soares Duarte Marques and Maria Emilia De Sousa

Received: 9 September 2022

Accepted: 19 October 2022

Published: 21 October 2022

Publisher's Note: MDPI stays neutral with regard to jurisdictional claims in published maps and institutional affiliations.



Copyright: © 2022 by the authors. Licensee MDPI, Basel, Switzerland. This article is an open access article distributed under the terms and conditions of the Creative Commons Attribution (CC BY) license (<https://creativecommons.org/licenses/by/4.0/>).

Abstract: Isoniazid (INH) is one of the key molecules employed in the treatment of tuberculosis (TB), the most deadly infectious disease worldwide. However, the efficacy of this cornerstone drug has seriously decreased due to emerging INH-resistant strains of *Mycobacterium tuberculosis* (*Mtb*). In the present study, we aimed to chemically tailor INH to overcome this resistance. We obtained thirteen novel compounds by linking INH to in-house synthesized sulfonate esters via a hydrazone bridge (**SIH1–SIH13**). Following structural characterization by FTIR, ¹H NMR, ¹³C NMR, and HRMS, all compounds were screened for their antitubercular activity against *Mtb* H37Rv strain and INH-resistant clinical isolates carrying *katG* and *inhA* mutations. Additionally, the cytotoxic effects of **SIH1–SIH13** were assessed on three different healthy host cell lines; HEK293, IMR-90, and BEAS-2B. Based on the obtained data, the synthesized compounds appeared as attractive antimycobacterial drug candidates with low cytotoxicity. Moreover, the stability of the hydrazone moiety in the chemical structure of the final compounds was confirmed by using UV/Vis spectroscopy in both aqueous medium and DMSO. Subsequently, the compounds were tested for their inhibitory activities against enoyl acyl carrier protein reductase (InhA), the primary target enzyme of INH. Although most of the synthesized compounds are hosted by the InhA binding pocket, **SIH1–SIH13** do not primarily show their antitubercular activities by direct InhA inhibition. Finally, in silico determination of important physicochemical parameters of the molecules showed that **SIH1–SIH13** adhered to Lipinski's rule of five. Overall, our study revealed a new strategy for modifying INH to cope with the emerging drug-resistant strains of *Mtb*.

Keywords: antimycobacterial; *Mycobacterium tuberculosis*; drug-resistant clinical isolates; molecular modeling; InhA

1. Introduction

Mycobacterium tuberculosis (*Mtb*) is the primary causative agent of the contagious disease tuberculosis (TB) that has devastated humankind for centuries [1]. TB is one of the leading infectious agent-related causes of mortality, as confirmed by the data presented in the latest World Health Organization (WHO) Global TB Report [2]. The successful control of TB by the current chemotherapeutic regimen, mainly consisting of four first-line drugs

(isoniazid, rifampicin, pyrazinamide, and ethambutol) [3], is often endangered by emerging drug-resistant *Mtb* strains [4].

Isoniazid (isonicotinic acid hydrazide, INH) is the cornerstone drug of modern TB therapy [5]. As a prodrug, INH needs to be oxidized by the enzyme catalase-peroxidase (KatG) to inhibit its biological target enoyl-acyl carrier protein reductase (InhA), a critical enzyme employed in the biosynthesis of mycolic acids [6,7]. Therefore, the clinical efficacy of INH in the treatment of drug-resistant TB is restricted due to mutations in *katG* or *inhA* and its promoter [8,9]. Furthermore, in humans, INH is metabolized and in this way deactivated by *N*-acetyltransferase type 2 (NAT2). This enzyme is responsible for the acetylation of the terminal nitrogen of the hydrazide group of INH using acetyl coenzyme A (acetyl-CoA) as the acetyl donor [10]. Due to genetic polymorphism in NAT2, variable acetylation rates arise, resulting in variations in blood drug concentrations among patients treated with INH [11]. These metabolic steps, which ultimately result in the activation and deactivation of INH, are schematically presented in Figure 1.

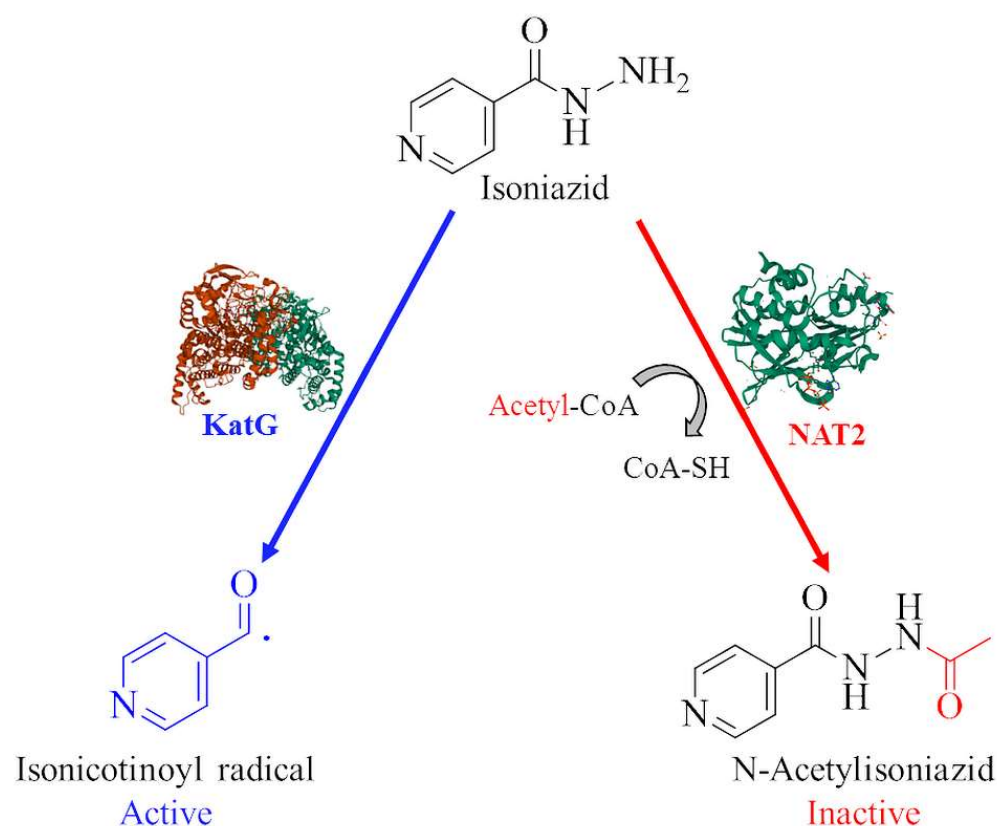


Figure 1. Schematic depiction of pathways leading to activation and inactivation of INH.

Due to their commonly reported anti-TB properties, hydrazone-possessing molecules are of considerable interest [12]. Particularly, the synthesis of hydrazone derivatives of the current anti-TB drugs such as isoniazid [13], ciprofloxacin [14], and pyrazinamide [15] is a frequently applied antimycobacterial drug design strategy (Figure 2). Therefore, hydrazone is considered to be an excellent linker fragment for newly-designed antitubercular agents.

As one of the most common ways to design and develop new drugs, molecular hybridization involves merging two or more pharmacophores in a single chemical entity, either directly or by using spacer units. The main goal of this strategy is to improve the biological profile while reducing side effects as much as possible [16,17].

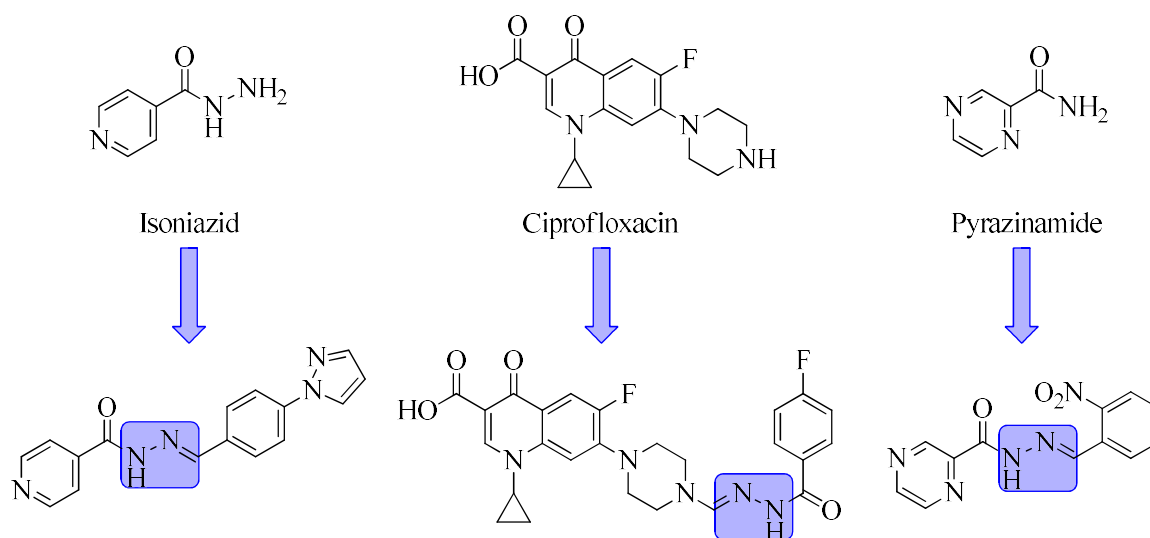


Figure 2. Biologically active hydrazone derivatives of marketed anti-TB drugs.

As previously indicated, INH is a significant component of the standardized regimens for TB treatment recommended by WHO. However, inappropriate treatment or poor patient compliance with the therapy often leads to the emergence of INH-resistant strains of *Mtb* [18]. Thus, tailoring the chemical structure of INH is accepted as a logical approach for designing new antitubercular compounds to overcome emerging resistance. Notably, modifications that allow INH to directly show its antimycobacterial effect without necessitating KatG activation or avoid the hydrazide functionality from acetylation can provide a new avenue for antitubercular drug development [19].

Prompted by these considerations, we set out with the goal of developing new antitubercular agents (**SIH1–SIH13**) by linking INH to various sulfonate esters that were also reported to exhibit antitubercular activities [20,21] via hydrazone bridge (Figure 3). When choosing the substituents on the sulfonate moiety, we mainly modified the *para* position of the terminal phenyl ring with various different groups including alkyl, aryl, acyl, halogen, and nitro. In this way, we made sure that the antitubercular activity was due to the substituent type independent from the position. Additionally, we carried out some additional chemical modifications (introducing two halogens, adding more alkyl groups, condensing phenyl to a heterocyclic ring, or changing the position of nitro group) to see how they will affect antimycobacterial activity and to establish preliminary structure-activity relationships for this class of compounds. Subsequently, we tested the antimycobacterial potency of these compounds against the reference *Mtb* strain H37Rv as well as against INH-resistant clinical isolates carrying *katG* and *inhA* promoter mutations.

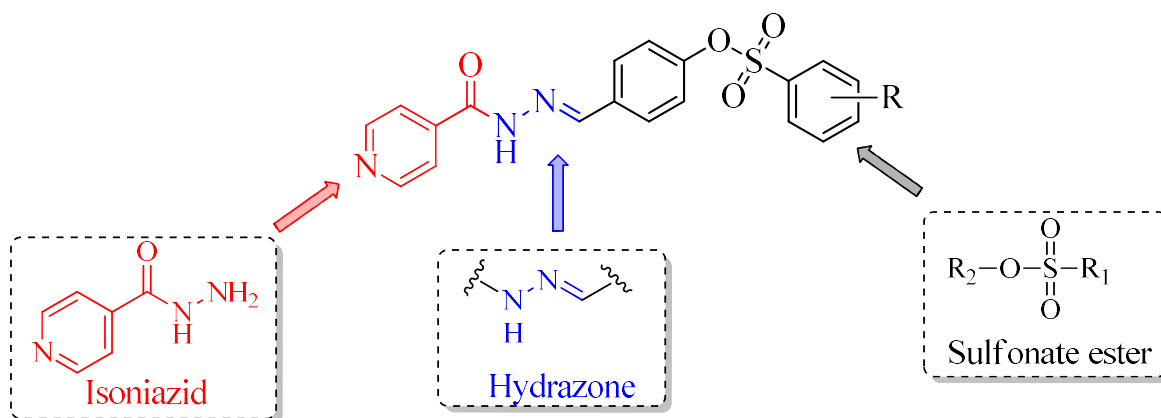
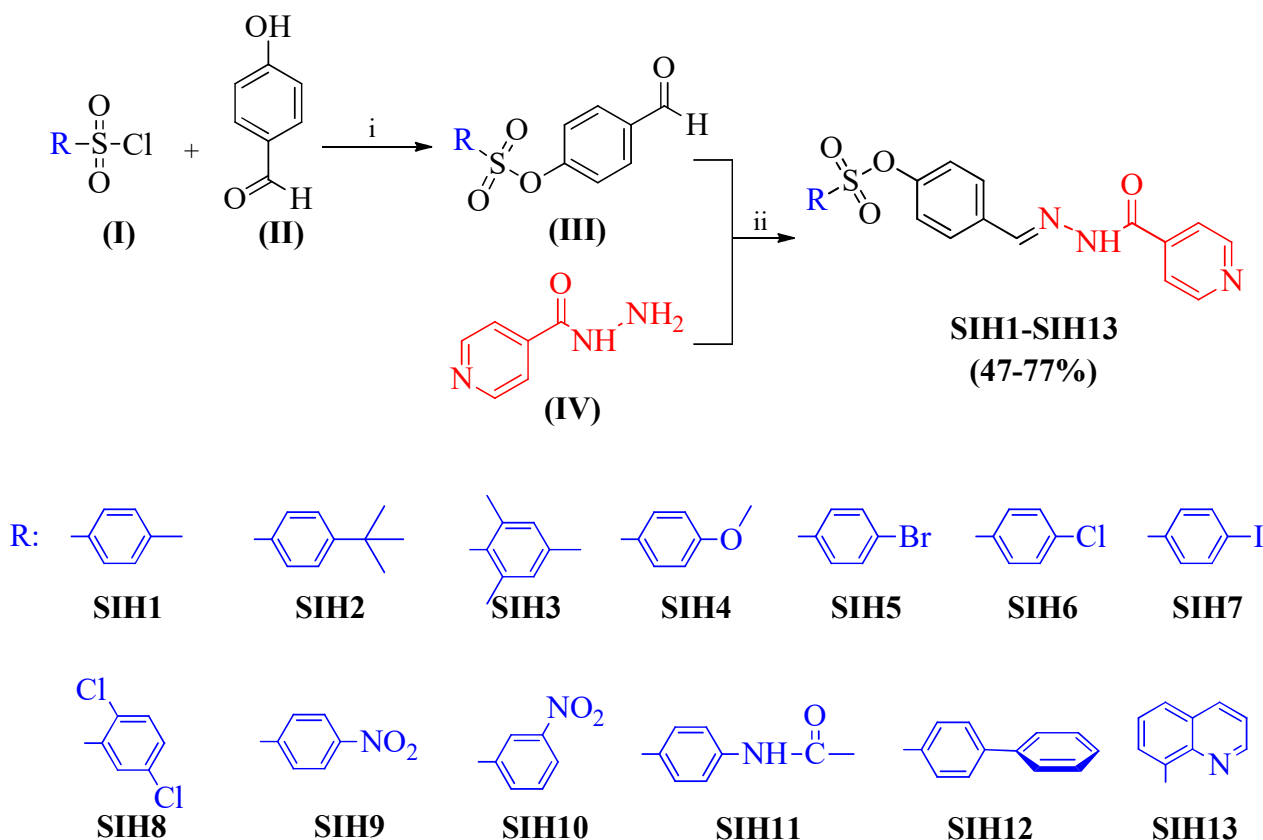


Figure 3. Design strategy of the studied molecules **SIH1–SIH13**.

2. Results and Discussion

2.1. Chemistry

The synthesis and chemical structures of the new isoniazid derivatives (**SIH1–SIH13**) are outlined in Scheme 1. The key intermediates, 4-formylphenyl benzenesulfonates, (**III**) were prepared through the reaction of aromatic sulfonyl chlorides (**I**) with 4-hydroxybenzaldehyde (**II**) in DMF in the presence of triethyl amine (TEA). Our target compounds (**SIH1–SIH13**) were obtained in 47–77% yield by refluxing 4-formylphenyl benzenesulfonates (**III**) and isoniazid (**IV**) in ethanol in the presence of a catalytic amount of glacial acetic acid.



Scheme 1. Reagents and conditions: (i) TEA/DMF, rt, (ii) EtOH/AcOH, reflux.

The structures of the newly synthesized compounds (**SIH1–SIH13**) were confirmed by their infrared (IR), ^1H NMR, ^{13}C NMR, and HRMS spectral data. In IR spectra, **SIH1–SIH13** were characterized by the appearance of absorption bands in the range of $3396\text{--}3248\text{ cm}^{-1}$, $1607\text{--}1596\text{ cm}^{-1}$, and $1676\text{--}1651\text{ cm}^{-1}$ due to N-H, C=N, and C=O stretching vibrations, respectively. Besides these, two characteristic bands for the SO_2 stretches were observed in the ranges of $1352\text{--}1335$ and $1143\text{--}1152\text{ cm}^{-1}$. Furthermore, ^1H NMR spectra of the compounds displayed two singlets at $12.21\text{--}12.11\text{ ppm}$ (O=C-NH) and $8.46\text{--}8.37\text{ ppm}$ (N=CH), respectively. According to the literature, the presence of a singlet downfield resonating ($8.46\text{--}8.37\text{ ppm}$) N=CH signal, exclusively accounts for the formation of *E*-isomers [22]. In addition, ^{13}C NMR spectra of the molecules showed a smaller number of resonances than the exact number of carbons due to the overlapped peaks in the aromatic field. The ^{13}C NMR spectra exhibit the C=O signal at $162.4\text{--}162.1\text{ ppm}$ and C=N signal at $140.7\text{--}140.8\text{ ppm}$, confirming the *N*-acylhydrazone skeleton in the chemical structures of **SIH1–SIH13**. ^1H NMR, ^{13}C NMR, HRMS, and FTIR spectra of the final compounds are provided in Supplementary Material.

2.2. Antitubercular Activity Evaluation and Cytotoxicity Assessment

We tested the antimycobacterial activity of all the compounds obtained against *Mtb* H37Rv and two INH-resistant clinical isolates (*katG* and *inhA* promoter mutants) by applying the Microplate Alamar Blue Assay (MABA) protocol. As toxicity to healthy host cells is a significant barrier to launching new antitubercular drugs, we additionally assessed the cytotoxicity of our compounds against three different cell lines: human embryonic kidney (HEK) 293, human lung cells IMR-90, and human epithelial bronchus cells BEAS-2B. Minimum inhibitory concentration (MIC) values against three *Mtb* strains tested as well as toxicity data of **SIH1–SIH13** are provided in Table 1.

Table 1. MIC values against *Mtb* H37Rv and INH-resistant clinical isolates, and cytotoxicity data of **SIH1–SIH13**.

| Compound | R | MIC (μM) | | | Toxicity * IC ₅₀ (μM) | | |
|------------------|-------------------------------|----------|--------------------------|--------------------------|----------------------------------|--------|---------|
| | | H37Rv | <i>inhA</i> ⁺ | <i>katG</i> ⁺ | HEK293 | IMR-90 | BEAS-2B |
| SIH1 | 4-methylphenyl | 0.31 | 1.56 | 50 | 57.21 | >100 | >100 |
| SIH2 | 4-(<i>tert</i> -butyl)phenyl | 0.62 | 1.56 | 25 | >100 | 89.50 | >100 |
| SIH3 | 2,4,6-trimethylphenyl | 0.62 | 6.25 | 50 | 100 | >100 | >100 |
| SIH4 | 4-methoxyphenyl | 0.31 | 1.56 | 6.25 | 40.76 | >100 | >100 |
| SIH5 | 4-bromophenyl | 0.62 | 3.12 | 25 | 100 | 90.32 | >100 |
| SIH6 | 4-chlorophenyl | 0.62 | 3.12 | >100 | >100 | >100 | >100 |
| SIH7 | 4-iodophenyl | 0.62 | 6.25 | >100 | >100 | 100 | >100 |
| SIH8 | 2,5-dichlorophenyl | 0.62 | 3.12 | 12.5 | >100 | 100 | >100 |
| SIH9 | 4-nitrophenyl | 0.62 | 3.12 | 25 | 100 | >100 | >100 |
| SIH10 | 3-nitrophenyl | 0.62 | 3.12 | 12.5 | >100 | >100 | >100 |
| SIH11 | 4-acetamidophenyl | 0.62 | 3.12 | 12.5 | >100 | >100 | >100 |
| SIH12 | 1,1'-biphenyl | 0.31 | 3.12 | 12.5 | 52.40 | 57.7 | >100 |
| SIH13 | quinoline-8-yl | 0.31 | 3.12 | 12.5 | 58.34 | 100 | >100 |
| Isoniazid | | 0.31 | 1.56 | 6.25 | NT | NT | NT |

NT: Not Tested, * experiments were performed in triplicate.

Based on the activity analyses, four compounds (**SIH1**, **SIH4**, **SIH12**, and **SIH13**) exhibited MIC values of 0.31 μM against *Mtb* H37Rv. The other molecules in this series were also efficient as antitubercular agents with MIC values of 0.62 μM. As expected, the MIC values of INH against two defined INH-resistant (*inhA* promoter mutant and *katG* S315T mutant) clinical isolates were found to be higher than the value obtained for INH-sensitive *Mtb* H37Rv. Against the *inhA* mutant INH-resistant *Mtb* clinical isolate, **SIH1**, **SIH2**, and **SIH4** were effective with MIC values of 1.56. Except for two compounds, **SIH5** and **SIH6** (MIC = 6.25 μM), the remaining compounds displayed antimycobacterial activity with MIC values of 3.12 μM. **SIH1–SIH13** were also screened against the other INH-resistant *Mtb* isolate with *katG* mutation. Among them, **SIH4** was the most effective compound with a MIC value of 6.25 μM which was the same value as calculated for INH. Excluding **SIH6** and **SIH7**, other molecules also represented antitubercular activity with MIC values ranging between 12.5 and 50 μM against *katG* mutant *Mtb* clinical isolate.

When the molecules were examined in terms of their chemical structures, it is noteworthy that **SIH4** with *p*-methoxy group on its phenyl ring was the most attractive compound showing the lowest MIC values against all the *Mtb* strains tested. Moreover, the other most active compounds against *Mtb* H37Rv carry a methyl (**SIH1**) or a phenyl (**SIH12**) group, or a condensed pyridine ring (**SIH13**) on their terminal phenyl rings. For the inhibition of *inhA* mutant *Mtb* strains, methyl (**SIH1**), *t*-butyl (**SIH2**), and methoxy (**SIH4**) on the *para* position of the phenyl ring were the most preferential substituents. As extensive molecular

modifications were carried out on the phenyl ring of sulfonate esters, it can be concluded that the changes in substituent types, positions, and volumes can easily be tolerated on this scaffold for antitubercular activity.

Furthermore, based on the cytotoxicity data obtained from the colorimetric MTT assay, the compounds were found to be non-toxic against lung cell lines IMR-90 and BEAS-2B. Only **SIH12** was slightly toxic towards IMR-90 with IC_{50} value of 57.7 μ M. Against HEK293, except for **SIH1**, **SIH4**, **SIH12**, and **SIH13** that were moderately toxic, our compounds did not present cytotoxicity. As TB predominantly is a respiratory disease, it is critical that we identified effective antimycobacterial drug candidates with favorable toxicity profiles, especially against the lung cells included in this study.

2.3. Stability Studies in Water and DMSO

Imine formations are well-known reversible condensation reactions [23]. Solvent type is one of the factors that need to be taken into account while assessing the stability of imines [24]. In the presence of water, the equilibrium may shift in favor of precursors and the target compounds to be tested in activity assays may be misinterpreted. Therefore, we tested the stability of our compounds under aqueous conditions to confirm the stability of the hydrazone functionality. In this way, we could make sure that the antitubercular activity of the molecules studied is not due to INH as one of the hydrolysis products of our compounds. Furthermore, the stability of the selected compounds was also assessed in DMSO, the solvent used in the biological experiments.

Accordingly, we performed stabilization tests for four selected compounds (**SIH1**, **SIH4**, **SIH12**, and **SIH13**) in both aqueous medium and DMSO by using UV/Vis spectroscopy. These representative compounds were selected based on their low MIC values against *Mtb* H37Rv strain. Samples with a concentration of 6.0×10^{-5} M were prepared in DMSO and a 28% ethanol-water mixture. The change in λ_{max} values throughout 24 h in the selected solvents was monitored to assess the stability of the hydrazone functionality. As expected, no significant change in λ_{max} values was observed for the compounds. UV/Vis absorption spectra of **SIH13** in DMSO and ethanol-water are provided in Figure 4. The results for **SIH1**, **SIH4**, and **SIH12** are reported in the Supplementary Material.

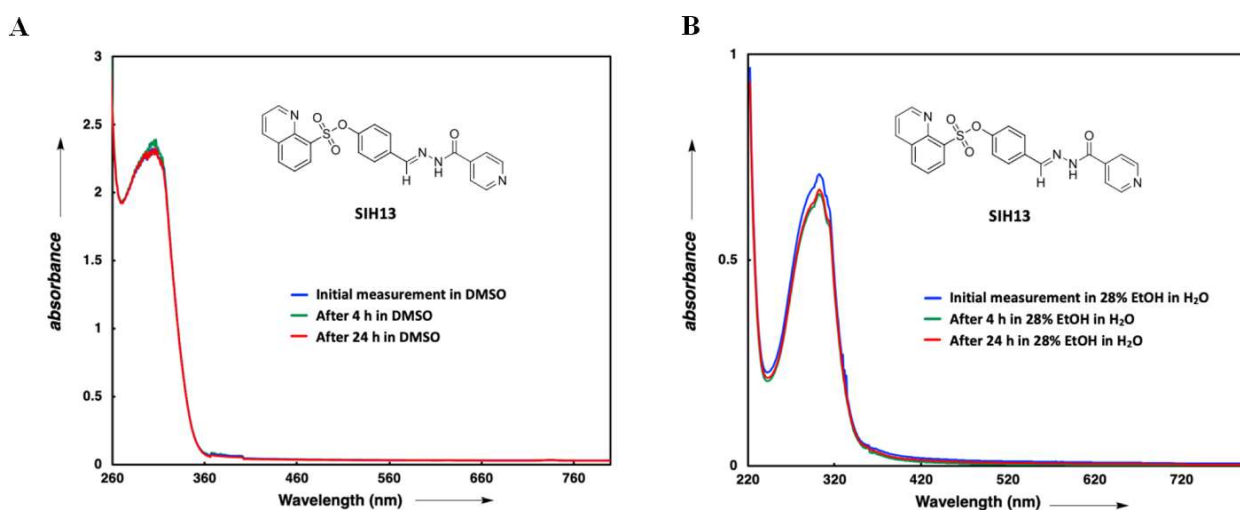


Figure 4. Stability assessment of **SIH13** in DMSO (A) and ethanol-water mixture (B).

2.4. *InhA* Inhibition

INH principally targets the *InhA* enzyme that is responsible for the biosynthesis of long-chain fatty acids in *Mtb*. Fatty acids, particularly mycolic acids, play a crucial role in the survival of *Mtb* since they are structural components of the bacterial cell wall [25]. Following the activation by KatG, INH produces a reactive isonicotinoyl-radical intermediate that quickly forms a covalent adduct with the *InhA* cofactor NADH [6]. As mutations in *katG*

reduce the activation of INH and thus yield the most prevalent type of INH resistance, developing direct InhA inhibitors that do not require KatG activation appears as an effective and rational strategy to overcome this resistance problem [26]. Therefore, we screened our INH-based compounds against InhA to determine if they show their antimycobacterial activity via direct inhibition of this enzyme (Table 2).

Table 2. Inhibitory results for **SIH1–SIH13** against InhA enzyme at 50 μ M concentration.

| Compound | % Inhibition | Compound | % Inhibition |
|-------------|--------------|--------------|--------------|
| SIH1 | 12 | SIH8 | NI |
| SIH2 | 25 | SIH9 | 8 |
| SIH3 | NI | SIH10 | 17 |
| SIH4 | 5 | SIH11 | 10 |
| SIH5 | 33 | SIH12 | 31 |
| SIH6 | 23 | SIH13 | 22 |
| SIH7 | 41 | TCL | 98 |

NI: No inhibition.

Although most of the molecules are recognized by the binding pocket of InhA, our compounds do not primarily represent their antitubercular activity by inhibiting InhA enzyme directly. **SIH7** was found to be a moderate inhibitor of InhA with 41% inhibition. As the main structural difference between the tested compounds is the substituent type and position on the phenyl ring of the sulfonate moiety, it is noteworthy that introducing iodine as a bulky and lipophilic halogen can be an important modification to bind to the active site of the enzyme. These data can be used useful for the design of effective antimycobacterial INH derivatives that are also capable of inhibiting InhA.

2.5. Molecular Modeling Studies

2.5.1. Molecular Docking

The active pocket of InhA is large enough to accommodate various direct inhibitors with different chemical scaffolds such as diphenyl ethers, 4-hydroxy-2-pyridones, benzamides, and thiadiazoles [27,28]. Despite this flexibility, in almost every case, the direct inhibitors block the enzyme via forming two key hydrogen bonds to Tyr158 and nicotinamide adenine dinucleotide (NAD) cofactor of InhA. Additional hydrophobic interactions are also required with the terminal lipophilic pockets of the binding site [29]. To rationalize the obtained data and explain the binding mode of our compounds to InhA, we carried out in silico studies. We docked **SIH7** into the binding pocket of InhA and compared its interactions to those of GEQ/Genz-10850, a direct inhibitor co-crystallized within the enzyme. The binding modes and the interactions of the compounds within the active pocket of InhA are provided in Supplementary Materials.

2.5.2. In Silico Prediction of Drug-Likeness

The unsuitable physicochemical profiles of drug candidate molecules can be a serious obstacle in the drug development process for the conversion of bioactive compounds into drugs. Thus, we performed theoretical calculations to identify drug-like properties of our compounds. We started with computing the descriptors that constitute the Lipinski's rule of five. This rule finds out if a chemical compound with preferable biological profile possesses suitable physicochemical properties that make it orally active in humans. Accordingly, to show oral bioavailability, a molecule should not breach more than one of the following requirements: molecular weight (MW) \leq 500, *n*-octanol/water partition coefficient ($\log P$) \leq 5, number of hydrogen bond donors (HBD) \leq 5 and number of hydrogen bond acceptors (HBA) \leq 10 [30]. Furthermore, we predicted the compounds' topological polar surface areas (TPSAs) and numbers of rotatable bonds (NRBs), both of which are regarded to be crucial characteristics for predicting the oral bioavailability of novel molecules [31]. The predicted physicochemical descriptors of **SIH1–SIH13** are presented in Table 3.

Table 3. Calculated molecular properties of **SIH1–SIH13**.

| Compound | MW ^a | LogP ^b | HBD ^c | HBA ^d | NRB ^e | TPSA ^f | Lipinski's Violation |
|--------------|-----------------|-------------------|------------------|------------------|------------------|-------------------|----------------------|
| SIH1 | 395.43 | 2.95 | 1 | 6 | 7 | 106.10 | 0 |
| SIH2 | 437.51 | 3.87 | 1 | 6 | 8 | 106.10 | 0 |
| SIH3 | 423.48 | 3.74 | 1 | 6 | 7 | 106.10 | 0 |
| SIH4 | 411.43 | 2.70 | 1 | 7 | 8 | 115.33 | 0 |
| SIH5 | 460.30 | 3.22 | 1 | 6 | 7 | 106.10 | 0 |
| SIH6 | 415.85 | 3.15 | 1 | 6 | 7 | 106.10 | 0 |
| SIH7 | 507.30 | 3.25 | 1 | 6 | 7 | 106.10 | 1 |
| SIH8 | 450.30 | 3.61 | 1 | 6 | 7 | 106.10 | 0 |
| SIH9 | 426.40 | 1.98 | 1 | 8 | 8 | 151.92 | 0 |
| SIH10 | 426.40 | 2.04 | 1 | 8 | 8 | 151.92 | 0 |
| SIH11 | 438.46 | 2.25 | 2 | 7 | 9 | 135.20 | 0 |
| SIH12 | 457.50 | 3.94 | 1 | 6 | 8 | 106.10 | 0 |
| SIH13 | 432.45 | 2.97 | 1 | 7 | 7 | 118.99 | 0 |

^a MW: molecular weight. ^b LogP: logarithm of *n*-octanol-water partition coefficient. ^c HBA: number of hydrogen bond acceptors. ^d HBD: number of hydrogen bond donors. ^e NRB: number of rotatable bonds. ^f TPSA: topological polar surface area.

Based on the estimated parameters, all compounds, except for **SIH7**, were shown to entirely follow Lipinski's rule of five. **SIH7** displays only one violation with a molecular weight of slightly more than 500. Furthermore, according to the calculated LogP values, the compounds are highly lipophilic compared to INH (LogP = −0.35, calculated in SwissADME). Besides mutations in either *katG* or the *inhA* promoter, this low hydrophobicity of INH is linked to the long duration of TB treatment [32]. The mycolic acid outer layer of *Mtb* is so lipophilic that INH cannot efficiently penetrate and cross it. The permeability of INH in the *Mtb* granuloma is also low due to its hydrophilic character [33]. Therefore, in this study, we succeeded in increasing the lipophilicity of INH with suitable chemical modifications to enhance its ability to diffuse through the cell membrane. The number of rotatable bonds, a significant descriptor of molecular flexibility, should be less than ten to keep conformational changes at minimum during the interactions with the biological targets. **SIH1–SIH13** follow this criterion as they all have ≤10 rotatable bonds. Additionally, TPSA of the compounds varied between 106.10 and 151.92 Å². Most of the clinically used drug molecules have TPSA less than 140–150 Å² [34], so our molecules stay in the acceptable range although the values calculated for **SIH9** and **SIH10** are slightly higher than 150 Å².

Consequently, the physicochemical properties of **SIH1–SIH13** support their potential position as relevant candidates in the antimycobacterial drug development process.

3. Material and Methods

3.1. Chemistry

3.1.1. Experimental

All the chemicals used in this study were purchased from commercial sources and were used without further purification. The completion of reactions and purities of the final compounds were monitored by thin layer chromatography (TLC) using Silica Gel 60 F254 TLC plate (Merck, Darmstadt, Germany). The *R_f* values of all the synthesized compounds were determined using ethyl acetate:*n*-hexane:methanol (7:2:1) as mobile phase. The melting points were determined by using Thomas Hoover Capillary Melting Point Apparatus (Philadelphia, PA, USA) and were uncorrected. Infrared (IR) spectra were obtained on Perkin Elmer Spectrum BX FT-IR (Beaconsfield, UK) and reported in the range of 4000–400 cm^{−1} using ATR accessory (Pike Technologies) with a diamond ATR crystal. The NMR spectra were recorded by Bruker spectrometer. ¹H NMR spectra were run at 400 MHz, while ¹³C NMR spectra were run at 100 MHz in deuterated dimethyl sulfoxide (DMSO-*d*₆). Chemical shifts (δ_{H}) and (δ_{C}) are expressed in values (ppm) using the solvent peak as the internal standard. All coupling constant (*J*) values are given in Hertz.

3.1.2. Synthesis

Preparation of aromatic aldehydes (III): Sulfonyl chlorides (1 mmol) and 4-hydroxybenzaldehyde (1.1 mmol) were mixed in DMF (20 mL) for 24 h at room temperature in the presence of triethylamine (1.35 mL). After pouring the mixture into ice, the resulting precipitate was filtered, washed with water, dried, and crystallized from ethanol [35].

General procedure for the synthesis of the target compounds SIH1–SIH13: A mixture of appropriate 4-formylphenyl substituted benzenesulfonate (0.5 mmol) and isoniazid (0.5 mmol) was refluxed with 5 drops of acetic acid in 15 mL methanol for 8 h. After completion of the reaction, the mixture was cooled and the precipitated solid was filtered, dried, and recrystallized from methanol (SIH1–SIH7, SIH11–SIH13) or methanol-ether (8:2) (SIH8–SIH10) [13].

3-((2-Isonicotinoylhydrazono)methyl)phenyl 4-methylbenzenesulfonate (SIH1): White solid, yield: 52% (205 mg). m.p. 209–210 °C. R_f (EtOAc:*n*-Hexane:MeOH = 7:2:1): 0.36. IR (ν , cm^{-1}): 3323 (N-H), 1676 (C=O), 1592 (C=N), 1371, and 1152 (SO_2 stretch). ^1H NMR (400 MHz, DMSO- d_6) δ 12.14 (s, 1H, -NH, D_2O exchangeable), 8.78 (d, $J = 4.5$ Hz, 2H, Ar-H), 8.42 (s, 1H, =CH), 7.81 (d, $J = 4.5$ Hz, 2H, Ar-H), 7.75 (d, $J = 8.0$ Hz, 4H, Ar-H), 7.48 (d, $J = 7.9$ Hz, 2H, Ar-H), 7.13 (d, $J = 8.4$ Hz, 2H, Ar-H), 2.42 (s, 3H, CH_3); ^{13}C NMR (100 MHz, DMSO- d_6) δ 162.2 (C=O), 150.8, 150.6, 147.9, 146.5, 140.8 (-C=N), 133.6, 131.6, 130.8, 129.3, 128.7, 123.1, 121.9, 21.6 (- CH_3); HRMS: m/z calcd for $\text{C}_{20}\text{H}_{17}\text{N}_3\text{O}_4\text{S}$ [$\text{M} + \text{H}$] $^+$: 396.1018; found 396.1015.

3-((2-Isonicotinoylhydrazono)methyl)phenyl 4-(*tert*-butyl)benzenesulfonate (SIH2): White solid, yield: 64% (280 mg). m.p. 182–183 °C. R_f (EtOAc:*n*-Hexane:MeOH = 7:2:1): 0.46. IR (ν , cm^{-1}): 3303 (N-H), 1663 (C=O), 1596 (C=N), 1365, and 1152 (SO_2 stretch). ^1H NMR (400 MHz, DMSO- d_6) δ 12.14 (s, 1H, -NH, D_2O exchangeable), 8.78 (d, $J = 4.6$ Hz, 2H, Ar-H), 8.43 (s, 1H, =CH), 7.82–7.80 (m, 4H, Ar-H), 7.76 (d, $J = 8.1$ Hz, 2H), 7.70 (d, $J = 8.3$ Hz, 2H), 7.15 (d, $J = 8.2$ Hz, 2H, Ar-H), 1.31 (s, 9H, CH_3); ^{13}C NMR (100 MHz, DMSO- d_6) δ 162.2 (C=O), 158.9, 150.8, 150.6, 148.0, 140.8 (-C=N), 133.6, 131.9, 129.3, 128.6, 127.2, 123.0, 122.0, 35.6 (-C-(CH_3) $_3$), 31.1 (- CH_3); HRMS: m/z calcd for $\text{C}_{23}\text{H}_{23}\text{N}_3\text{O}_4\text{S}$ [$\text{M} + \text{H}$] $^+$: 438.1488; found 438.1482.

3-((2-Isonicotinoylhydrazono)methyl)phenyl 2,4,6-trimethylbenzenesulfonate (SIH3): Yellow solid, yield: 47% (199 mg). m.p. 108–109 °C. R_f (EtOAc:*n*-Hexane:MeOH = 7:2:1): 0.43. IR (ν , cm^{-1}): 3396 (N-H), 1661 (C=O), 1600 (C=N), 1360, and 1152 (SO_2 stretch). ^1H NMR (400 MHz, DMSO- d_6) δ 12.13 (s, 1H, -NH, D_2O exchangeable), 8.78 (d, $J = 4.4$ Hz, 2H, Ar-H), 8.41 (s, 1H, =CH), 7.80 (d, $J = 4.6$ Hz, 2H, Ar-H), 7.74 (d, $J = 8.0$ Hz, 2H, Ar-H), 7.16 (s, 2H, Ar-H), 7.09 (d, $J = 8.1$ Hz, 2H, Ar-H), 2.48 (s, 6H, CH_3), 2.31 (s, 3H, - CH_3); ^{13}C NMR (100 MHz, DMSO- d_6) δ 162.2 (C=O), 150.8, 150.4, 148.0, 144.9, 140.8 (-C=N), 140.3, 133.6, 132.4, 129.8, 129.3, 122.9, 121.9, 22.6 (2x- CH_3), 21.06 (- CH_3); HRMS: m/z calcd for $\text{C}_{22}\text{H}_{21}\text{N}_3\text{O}_4\text{S}$ [$\text{M} + \text{H}$] $^+$: 424.1331; found 424.1323.

3-((2-Isonicotinoylhydrazono)methyl)phenyl 4-methoxybenzenesulfonate (SIH4): White solid, yield: 71% (296 mg). m.p. 194–195 °C. R_f (EtOAc:*n*-Hexane:MeOH = 7:2:1): 0.33. IR (ν , cm^{-1}): 3288 (N-H), 1665 (C=O), 1596 (C=N), 1369, and 1152 (SO_2 stretch). ^1H NMR (400 MHz, DMSO- d_6) δ 12.14 (s, 1H, -NH, D_2O exchangeable), 8.78 (d, $J = 4.5$ Hz, 2H, Ar-H), 8.43 (s, 1H, =CH), 7.74–7.81 (m, 6H, Ar-H), 7.17 (d, $J = 8.2$ Hz, 2H, Ar-H), 7.12 (d, $J = 8.1$ Hz, 2H, Ar-H), 3.87 (s, 3H, - OCH_3); ^{13}C NMR (100 MHz, DMSO- d_6) δ 164.6, 162.2 (C=O), 150.8, 150.0, 148.0, 140.8 (-C=N), 133.6, 131.2, 129.3, 125.8, 123.2, 121.9, 115.5, 56.4 (- OCH_3); HRMS: m/z calcd for $\text{C}_{20}\text{H}_{17}\text{N}_3\text{O}_5\text{S}$ [$\text{M} + \text{H}$] $^+$: 412.0967; found 412.0959.

3-((2-Isonicotinoylhydrazono)methyl)phenyl 4-bromobenzenesulfonate (SIH5): White solid, yield: 61% (279 mg). m.p. 217–218 °C. R_f (EtOAc:*n*-Hexane:MeOH = 7:2:1): 0.42. IR (ν , cm^{-1}): 3306 (N-H), 1673 (C=O), 1599 (C=N), 1379, and 1150 (SO_2 stretch). ^1H NMR (400 MHz, DMSO- d_6) δ 12.15 (s, 1H, -NH, D_2O exchangeable), 8.78 (d, $J = 4.4$ Hz, 2H, Ar-H), 8.43 (s, 1H, =CH), 7.90 (d, $J = 7.7$ Hz, 2H, Ar-H), 7.81–7.77 (m, 6H, Ar-H), 7.16 (d, $J = 7.9$ Hz, 2H, Ar-H); ^{13}C NMR (100 MHz, DMSO- d_6) δ 162.2 (C=O), 150.8, 150.4,

147.9, 140.8 (-C=N), 133.9, 133.8, 133.5, 130.6, 129.9, 129.4, 123.1, 121.9, HRMS: m/z calcd for $C_{19}H_{14}BrN_3O_4S$ $[M + H]^+$: 459.9967; found 459.9965.

3-((2-Isonicotinoylhydrazono)methyl)phenyl 4-chlorobenzenesulfonate (SIH6): Yellow solid, yield: 55% (228 mg). m.p. 210–211 °C. R_f (EtOAc:*n*-Hexane:MeOH = 7:2:1): 0.43. IR (ν , cm^{-1}): 3357 (N-H), 1665 (C=O), 1602 (C=N), 1368, and 1149 (SO₂ stretch). ¹H NMR (400 MHz, DMSO-*d*₆) δ 12.15 (s, 1H, -NH, D₂O exchangeable), 8.78 (d, J = 4.9 Hz, 2H, Ar-H), 8.43 (s, 1H, =CH), 7.89 (d, J = 8.1 Hz, 2H, Ar-H), 7.82–7.75 (m, 6H, Ar-H), 7.16 (d, J = 7.9 Hz, 2H, Ar-H); ¹³C NMR (100 MHz, DMSO-*d*₆) δ 162.2 (C=O), 150.8, 150.4, 147.9, 140.8 (-C=N), 140.7, 133.9, 133.4, 130.7, 130.6, 129.4, 123.1, 121.9; HRMS: m/z calcd for $C_{19}H_{14}ClN_3O_4S$ $[M + H]^+$: 416.0472; found 416.0463.

3-((2-Isonicotinoylhydrazono)methyl)phenyl 4-iodobenzenesulfonate (SIH7): Pale yellow solid, yield: 65% (329 mg). m.p. 240–241 °C. R_f (EtOAc:*n*-Hexane:MeOH = 7:2:1): 0.44. IR (ν , cm^{-1}): 3263 (N-H), 1660 (C=O), 1599 (C=N), 1378, and 1151 (SO₂ stretch). ¹H NMR (400 MHz, DMSO-*d*₆) δ 12.15 (s, 1H, -NH, D₂O exchangeable), 8.78 (d, J = 4.1 Hz, 2H, Ar-H), 8.43 (s, 1H, =CH), 8.07 (d, J = 7.2 Hz, 2H, Ar-H), 7.82–7.76 (m, 4H, Ar-H), 7.62 (d, J = 7.7 Hz, 2H, Ar-H), 7.16 (d, J = 7.9 Hz, 2H, Ar-H); ¹³C NMR (100 MHz, DMSO-*d*₆) δ 162.2 (C=O), 150.8, 150.4, 147.9, 140.8 (-C=N), 139.3, 134.1, 133.9, 130.1, 129.4, 123.1, 121.9, 104.9; HRMS: m/z calcd for $C_{19}H_{14}IN_3O_4S$ $[M + H]^+$: 507.9828; found 507.9814.

3-((2-Isonicotinoylhydrazono)methyl)phenyl 2,5-dichlorobenzenesulfonate (SIH8): Yellow solid, yield: 59% (265 mg). m.p. 177–178 °C. R_f (EtOAc:*n*-Hexane:MeOH = 7:2:1): 0.42. IR (ν , cm^{-1}): 3303 (N-H), 1667 (C=O), 1598 (C=N), 1390, and 1143 (SO₂ stretch). ¹H NMR (400 MHz, DMSO-*d*₆) δ 12.21 (s, 1H, -NH, D₂O exchangeable), 8.78 (d, J = 4.8 Hz, 2H, Ar-H), 8.46 (s, 1H, =CH), 7.93–7.78 (m, 7H, Ar-H), 7.25 (d, J = 8.3 Hz, 2H, Ar-H); ¹³C NMR (100 MHz, DMSO-*d*₆) δ 162.2 (C=O), 150.8, 150.1, 147.9, 140.7 (-C=N), 136.9, 134.8, 134.1, 133.2, 131.7, 131.2, 129.6, 122.7, 122.0, 121.5; HRMS: m/z calcd for $C_{19}H_{13}Cl_2N_3O_4S$ $[M + H]^+$: 450.0082; found 450.0076.

3-((2-Isonicotinoylhydrazono)methyl)phenyl 4-nitrobenzenesulfonate (SIH9): White solid, yield: 77% (328 mg). m.p. 211–212 °C. R_f (EtOAc:*n*-Hexane:MeOH = 7:2:1): 0.51. IR (ν , cm^{-1}): 3248 (N-H), 1663 (C=O), 1602 (C=N), 1379, and 1147 (SO₂ stretch). ¹H NMR (400 MHz, DMSO-*d*₆) δ 12.17 (s, 1H, -NH, D₂O exchangeable), 8.78 (d, J = 4.5 Hz, 2H, Ar-H), 8.46 (d, J = 8.3 Hz, 2H, Ar-H), 8.43 (s, 1H, =CH), 8.17 (d, J = 8.1 Hz, 2H, Ar-H), 7.81–7.77 (m, 4H, Ar-H), 7.18 (d, J = 8.0 Hz, 2H, Ar-H); ¹³C NMR (100 MHz, DMSO-*d*₆) δ 162.4 (C=O), 151.6, 150.8, 150.2, 148.0, 140.7 (-C=N), 139.7, 133.9, 130.5, 129.6, 125.5, 123.1, 122.0; HRMS: m/z calcd for $C_{19}H_{14}N_4O_6S$ $[M + H]^+$: 427.0707; found 427.0685.

3-((2-Isonicotinoylhydrazono)methyl)phenyl 3-nitrobenzenesulfonate (SIH10): White solid, yield: 64% (264 mg). m.p. 203–204 °C. R_f (EtOAc:*n*-Hexane:MeOH = 7:2:1): 0.58. IR (ν , cm^{-1}): 3267 (N-H), 1651 (C=O), 1607 (C=N), 1379, and 1148 (SO₂ stretch). ¹H NMR (400 MHz, DMSO-*d*₆) δ 12.17 (s, 1H, -NH, D₂O exchangeable), 8.78 (d, J = 4.8 Hz, 2H, Ar-H), 8.66 (d, J = 8.0 Hz, 1H, Ar-H), 8.50 (s, 1H, Ar-H), 8.43 (s, 1H, =CH), 8.29 (d, J = 8.1 Hz, 1H, Ar-H), 7.97 (t, J = 8.0 Hz, 1H, Ar-H), 7.81–7.76 (m, 4H, Ar-H), 7.22 (d, J = 8.1 Hz, 2H, Ar-H); ¹³C NMR (100 MHz, DMSO-*d*₆) δ 162.2 (C=O), 150.8, 150.2, 148.6, 147.9, 140.8 (-C=N), 135.8, 134.6, 134.1, 132.5, 130.2, 129.5, 123.5, 123.3, 122.0; HRMS: m/z calcd for $C_{19}H_{14}N_4O_6S$ $[M + H]^+$: 427.0707; found 427.0682.

3-((2-Isonicotinoylhydrazono)methyl)phenyl 4-acetamidobenzenesulfonate (SIH11): White solid, yield: 68% (298 mg). m.p. 193–194 °C. R_f (EtOAc:*n*-Hexane:MeOH = 7:2:1): 0.35. IR (ν , cm^{-1}): 3257 (N-H), 1670 (C=O), 1597 (C=N), 1352, and 1147 (SO₂ stretch). ¹H NMR (400 MHz, DMSO-*d*₆) δ 12.13 (s, 1H, -NH, D₂O exchangeable) 10.50 (s, 1H, -NH), 8.77 (d, J = 3.8 Hz, 2H, Ar-H), 8.42 (s, 1H, =CH), 7.82–7.74 (m, 8H, Ar-H), 7.12 (d, J = 8.0 Hz, 2H, Ar-H), 2.10 (s, 3H, -CH₃); ¹³C NMR (100 MHz, DMSO-*d*₆) δ 169.9 (C=O), 162.2 (C=O), 150.8, 150.6, 148.1, 145.5, 140.8 (-C=N), 133.6, 130.2, 129.3, 127.5, 123.2, 121.9, 119.2, 24.7 (-CH₃); HRMS: m/z calcd for $C_{21}H_{18}N_4O_5S$ $[M + H]^+$: 439.1076; found 439.1066.

3-((2-Isonicotinoylhydrazono)methyl)phenyl [1,1'-biphenyl]-4-sulfonate (SIH12): Orange solid, yield: 53% (242 mg). m.p. 118–119 °C. R_f (EtOAc:*n*-Hexane:MeOH = 7:2:1): 0.44. IR (ν , cm^{-1}): 3382 (N-H), 1660 (C=O), 1596 (C=N), 1372, and 1151 (SO₂ stretch). ¹H

NMR (400 MHz, DMSO- d_6) δ 12.16 (s, 1H, -NH, D₂O exchangeable), 8.78 (d, J = 4.7 Hz, 2H, Ar-H), 8.43 (s, 1H, =CH), 8.00–7.94 (m, 4H, Ar-H), 7.81–7.77 (m, 5H, Ar-H), 7.55–7.45 (m, 4H, Ar-H), 7.19 (d, J = 8.3 Hz, 2H, Ar-H); ¹³C NMR (100 MHz, DMSO- d_6) δ 162.2 (C=O), 150.8, 150.5, 148.0, 146.8, 140.8 (-C=N), 138.2, 133.7, 133.2, 129.7, 129.6, 129.4, 128.3, 127.7, 127.5, 123.6, 121.9; HRMS: m/z calcd for C₂₅H₁₉N₃O₄S [M + H]⁺: 458.1175; found 458.1166.

3-((2-Isonicotinoylhydrazono)methyl)phenyl quinoline-8-sulfonate (SIH13): White solid, yield: 72% (327 mg). m.p. 231–232 °C. R_f (EtOAc:*n*-Hexane:MeOH = 7:2:1): 0.22. IR (ν , cm⁻¹): 3294 (N-H), 1670 (C=O), 1598 (C=N), 1359, and 1142 (SO₂ stretch). ¹H NMR (400 MHz, DMSO- d_6) δ 12.11 (s, 1H, -NH, D₂O exchangeable), 9.23 (s, 1H, Ar-H), 8.77 (d, linebreak emphj = 4.2 Hz, 2H, Ar-H), 8.64 (d, J = 8.2 Hz, 1H, Ar-H), 8.47 (d, J = 8.1 Hz, 1H, Ar-H), 8.39 (d, J = 4.9 Hz, 1H, Ar-H), 8.37 (s, 1H, =CH), 7.82–7.77 (m, 4H, Ar-H), 7.68 (d, J = 8.2 Hz, 2H, Ar-H), 7.10 (d, J = 8.2 Hz, 2H, Ar-H); ¹³C NMR (100 MHz, DMSO- d_6) δ 162.1 (C=O), 152.9, 150.9, 150.8, 148.0, 143.5, 140.8 (-C=N), 137.7, 136.9, 134.5, 133.4, 131.7, 129.2, 126.2, 123.6, 122.9, 122.5, 121.9; HRMS: m/z calcd for C₂₂H₁₆N₄O₄S [M+Na]⁺: 455.0790; found 455.0788.

3.2. Microplate Alamar Blue Assay (MABA) Protocol

Mycobacterium tuberculosis H37Rv (*Mtb*) obtained from the American Type Culture Collection (ATCC) and drug-resistant clinical isolates from Oslo University Hospital were streaked onto 7H10+OADC agar plates and incubated at 37 °C. In OADC-enriched liquid Middlebrook 7H9 medium, pure colonies from agar plates were grown to the middle of the log phase. Subsequently, *Mtb* cultures were exponentially grown and inoculated into Middlebrook 7H9 medium on 96-well plates at progressively higher concentrations of the testing chemicals, with approximately 4 × 10⁵ CFU/mL in 200 μ L of each well. Before receiving 32.5 μ L of a resazurin-tween mixture (8:5 ratio of 0.6 mM Resazurin in 1 × PBS to 20% Tween 80), plates were incubated at 37 °C for one week. The production of fluorescent resorufin assists in determining the minimum inhibitory concentration (MIC) of the compounds tested [13].

3.3. Cytotoxicity Protocol

The MTT (3-(4,5-dimethylthiazol-2-yl)-2,5-diphenyltetrazolium bromide) test was used to assess the cytotoxicity of the compounds against the cell lines Human Embryonic Kidney cells (HEK 293), Normal Lung Fibroblasts (IMR-90), and Human non-tumorigenic lung epithelial cells (BEAS-2B). All cell lines were obtained from ATCC. When testing compounds **SIH1–SIH13**, they were added by the use of double dilution across 6 dosages ranging from 100 μ M to 3.12 μ M to a sterile 96 well microtiter plate containing 1 × 10⁴ cells/well and cultured for 48 h at 37 °C with 5% CO₂. The medium was removed, and 10 μ L of MTT reagent (5 mg/mL) was added to the wells and incubated for another 3 h. The MTT reagent was then removed, and 100 μ L of DMSO was added into each well. DMSO dissolves the formazan crystals that have formed in the wells. The absorbance was measured at 580 nm against a blank using the Thermo Scientific variaskan lux microplate reader, and the IC₅₀ values were calculated by using GraphPad Prism [36,37].

3.4. Stability Studies

The T80+ series of UV/Vis Spectrophotometers (PG Instruments Ltd.) were used for stability assessment studies. The stability experiments were performed at 25 °C with wavelength ranges of 260–800 nm. DMSO and EtOH were purchased as reagent grade and used without any purification. Samples with a concentration of 6.0 × 10⁻⁵ M were prepared in DMSO and EtOH-water. The change in λ_{\max} values throughout the 24 h in the selected solvents was monitored to assess the stability of the hydrazone moieties.

3.5. *InhA* Inhibition

3.5.1. Production and Purification of *InhA*

InhA sequence (UniProtKB: P9WGR1) has been optimized for *Escherichia coli* BL21 DE3 strain with GenSmart™ Codon Optimization (GenScript) and inserted in pET15b plasmid using the NdeI and BamHI restriction sites. BL21 (DE3) strains have been transformed with pET15b-*InhA* plasmid. A colony from this transformation was grown in LB medium containing 100 mg/mL ampicillin at 37 °C 180 rpm overnight. Then, 10 mL of this solution was added to 990 mL of LB medium containing ampicillin (100 mg/mL) and incubated at 37 °C 150 rpm until an optical density (OD) at 600 nm of 0.6–0.8 was reached. Once the OD₆₀₀ was reached, 1 mL of 1 M isopropyl β-D-1-thiogalactopyranoside (IPTG) was added and the solution was incubated at 30 °C for 4 h at 150 rpm. Bacteria cells were collected by centrifugation at 6000 × *g* for 30 min at 4 °C. Cells from pellets were solubilized with buffer (20 mM Tris-HCl, 300 mM NaCl, 10 mM imidazole, pH 7.9) and lysed using an Emulsiflex-C5 cell disruptor (Avestin). The lysate was centrifuged at 25,000 × *g* for 30 min at 4 °C, the supernatant was filtered off with a 0.2 μm filter and injected into a nickel-chelated Hi-Trap HP 1 mL (Cytiva) column previously equilibrated with washing buffer (20 mM Tris-HCl, 300 mM NaCl, 10 mM imidazole, pH 7.9). After washing out the unbound proteins, bound His6-*InhA* was eluted using a buffer with higher imidazole concentration (20 mM Tris-HCl, 300 mM NaCl, 300 mM imidazole, pH 7.9). Fractions corresponding to His6-*InhA* were pooled together and concentrated using centrifugal concentrator (Vivaspin 10,000 MWCO). Then, the concentrated protein solution was centrifuged at 10,000 × *g* for 10 min at 4 °C to remove aggregates and injected into a SepFast 16/60 6–600 kDa pg column (BioToolomics) previously equilibrated with buffer (30 mM PIPES, 150 mM NaCl, pH 6.8). Fractions corresponding to His6-*InhA* were pooled together then aliquots of 200 μL at 5 μM were prepared followed by flash freezing in liquid nitrogen. Frozen His6-*InhA* proteins were stored at –80 °C until usage.

3.5.2. Enzymatic Assay

InhA activity assays were monitored by following NADH concentration at 340 nm with a Cary 300 UV-vis (Agilent) spectrophotometer. As described previously [38], 2-trans-dodecenoyl-CoA (DDCoA) was used as an analogue of the substrate for this reaction. Briefly, to 840 μL of buffer (30 mM PIPES, 150 mM NaCl, pH 6.8) in 1 mL cuvette, inhibitor in DMSO at constant 5% *v/v* of DMSO (50 μL), 50 μL DDCoA of 1 mM stock in buffer and 50 μL of NADH (Alfa Aesar) of 5 mM stock in buffer were added. After a short period of 2 min pre-incubation at 25 °C, the reaction was started by the addition of 10 μL His6-*InhA* from a 5 μM stock solution prepared as explained before. Rate of NADH oxidation during His6-*InhA* activity is monitored in the presence or in the absence of inhibitor. The inhibitory activity of tested molecules is expressed as the percentage inhibition of His6-*InhA* activity (with respect to control reaction) without inhibitor, as shown below. All activity assays were performed in duplicate or triplicate.

$$\text{inhibition \%} = \frac{\text{Reference slope} - \text{Compound slope}}{\text{Reference slope}} \times 100$$

3.6. *In Silico* Studies

3.6.1. Molecular Docking

The 3D crystal structure of *Mycobacterium tuberculosis* enoyl-ACP reductase (*InhA*) with its native inhibitor GEQ, (4-(9*H*-fluoren-9-yl)piperazin-1-yl)(1*H*-indol-5-yl)methanone, was downloaded from Protein Data Bank under the PDB Code 1P44 [39]. The chemical structure of **SIH7** showing the best inhibition value against *InhA* among the tested compounds was sketched and MMFF94 force field in LigandScout 4.4 was used to minimize the energy of the 3D structure [40]. **SIH7** was docked into the binding pocket of *InhA* with default parameters of AutoDock [41], implemented in LigandScout 4.4. The obtained modes were

ranked based on their estimated binding energies and the figures of the most plausible binding pose were generated using LigandScout and Maestro [42].

3.6.2. Prediction of Drug-Likeness

The chemical structures of all compounds were drawn and their significant parameters were predicted by using SwissADME [43].

4. Conclusions

The rapid emergence and global spread of drug-resistant strains of *Mtb* have once again made TB an urgent concern to human health around the world. Particularly, the resistance developed against INH, as the frontline drug of TB treatment, has appeared as a significant handicap to controlling the global prevalence of the disease. In this study, we focused on the chemical modifications of inexpensive INH to provide a new route towards the antitubercular drug development process. Accordingly, we synthesized new INH derivatives by linking this scaffold to sulfonate esters with a hydrazone functionality (**SIH1–SIH13**). We established the stability of the compounds both in DMSO and water to eliminate the possibility that the antitubercular effect was due to INH released by hydrolyzation during biological experiments. The antitubercular and toxicity data obtained from MABA and MTT assays respectively confirmed the potential of the compounds in TB treatment. Testing the inhibitory activity of **SIH1–SIH13** against InhA, the primary target of INH, showed that our compounds can be hosted within the binding pocket of the enzyme. However, the antimycobacterial activity was not mainly due to InhA inhibition. Calculating some critical physicochemical descriptors of the compounds confirmed their drug-likeness and emphasized the importance of the increased lipophilicity in the biological profile of **SIH1–SIH13** as compared to INH. Altogether, our study presented a new approach for modifying INH to overcome the challenging drug resistance problem in TB treatment.

Supplementary Materials: The following supporting information can be downloaded at: <https://www.mdpi.com/article/10.3390/ph15101301/s1>, ¹H NMR, ¹³C NMR, FTIR, and HRMS spectra of all synthesized compounds, InhA optimised sequence, UV/Vis spectra of **SIH1**, **SIH4**, and **SIH12** in DMSO and EtOH-water, and molecular docking figures and discussion are provided.

Author Contributions: Conceptualization, Ş.D.D. and M.G.G.; Investigation, E.K.A., M.İ.H., V.S.K., R.T. and C.D.; Data curation, E.K.A., M.İ.H., V.S.K. and R.T.; Formal analysis, E.K.A., M.İ.H., V.S.K., R.T. and C.D.; Supervision, Ş.D.D., M.G.G., C.L., L.M. and T.T.; Funding acquisition, T.T. and M.G.G.; Writing original draft, M.İ.H., E.K.A., M.G.G., C.D., V.S.K. and R.T.; Writing-review & editing, Ş.D.D., C.L., L.M., T.T. and M.G.G. All authors have read and agreed to the published version of the manuscript.

Funding: T.T. acknowledges the financial support provided by the Research Council of Norway (RCN project numbers #234506, #261669 and #309592) and JPIAMR (RCN project number #298410). M.G.G. acknowledges the financial support provided by the BAGEP Award of the Science Academy.

Institutional Review Board Statement: Not applicable.

Informed Consent Statement: Not applicable.

Data Availability Statement: Data are contained within the article or Supplementary Materials.

Acknowledgments: M.G.G. also would like to thank Gerhard Wolber, Freie Universität Berlin, for providing the license for LigandScout 4.4. RT thanks Université Fédérale Toulouse Midi-Pyrénées and Occitanie region for PhD grant.

Conflicts of Interest: The authors declare no conflict of interest.

References

1. Migliori, G.B.; Ong, C.W.M.; Petrone, L.; D'ambrosio, L.; Centis, R.; Goletti, D. The definition of tuberculosis infection based on the spectrum of tuberculosis disease. *Breathe* **2021**, *17*, 210079. [CrossRef] [PubMed]
2. WHO Global Tuberculosis Report. 2020. Available online: <https://www.who.int/teams/global-tuberculosis-programme/tb-reports/global-tuberculosis-report-2020> (accessed on 5 June 2022).
3. Pontali, E.; Raviglione, M.C.; Migliori, G.B.; Akkerman, O.W.; Alffenaar, J.W.; Blanc, F.X.; Borisov, S.; Cirillo, D.M.; Dalcolmo, M.; Dheda, K.; et al. Regimens to treat multidrug-resistant tuberculosis: Past, present and future perspectives. *Eur. Respir. Rev.* **2019**, *28*, 190035. [CrossRef] [PubMed]
4. Khawbung, J.L.; Nath, D.; Chakraborty, S. Drug resistant Tuberculosis: A review. *Comp. Immunol. Microbiol. Infect. Dis.* **2021**, *74*, 101574. [CrossRef] [PubMed]
5. Vilchèze, C.; Jacobs, W.R. The Isoniazid Paradigm of Killing, Resistance, and Persistence in Mycobacterium tuberculosis. *J. Mol. Biol.* **2019**, *431*, 3450–3461. [CrossRef] [PubMed]
6. Reingewertz, T.H.; Meyer, T.; McIntosh, F.; Sullivan, J.; Meir, M.; Chang, Y.F.; Behr, M.A.; Barkana, D. Differential sensitivity of mycobacteria to isoniazid is related to differences in katG-mediated enzymatic activation of the drug. *Antimicrob. Agents Chemother.* **2020**, *64*, e01899-19. [CrossRef]
7. de Ávila, M.B.; Bitencourt-Ferreira, G.; de Azevedo, W.F. Structural Basis for Inhibition of Enoyl-[Acyl Carrier Protein] Reductase (InhA) from Mycobacterium tuberculosis. *Curr. Med. Chem.* **2018**, *27*, 745–759. [CrossRef]
8. Bollela, V.R.; Namburete, E.I.; Feliciano, C.S.; Macheque, D.; Harrison, L.H.; Caminero, J.A. Detection of katG and inhA mutations to guide isoniazid and ethionamide use for drug-resistant tuberculosis. *Int. J. Tuberc. Lung Dis.* **2016**, *20*, 1099–1104. [CrossRef]
9. Belete, T.M. Recent Progress in the Development of Novel Mycobacterium Cell Wall Inhibitor to Combat Drug-Resistant Tuberculosis. *Microbiol. Insights* **2022**, *15*, 117863612210998. [CrossRef]
10. Upton, A.M.; Mushtaq, A.; Victor, T.C.; Sampson, S.L.; Sandy, J.; Smith, D.-M.; van Helden, P.V.; Sim, E. Arylamine N-acetyltransferase of Mycobacterium tuberculosis is a polymorphic enzyme and a site of isoniazid metabolism. *Mol. Microbiol.* **2001**, *42*, 309–317. [CrossRef]
11. Kinzig-Schippers, M.; Tomalik-Scharte, D.; Jetter, A.; Scheidel, B.; Jakob, V.; Rodamer, M.; Cascorbi, I.; Doroshenko, O.; Sörgel, F.; Fuhr, U. Should we use N-acetyltransferase type 2 genotyping to personalize isoniazid doses? *Antimicrob. Agents Chemother.* **2005**, *49*, 1733–1738. [CrossRef]
12. Sharma, P.C.; Sharma, D.; Sharma, A.; Saini, N.; Goyal, R.; Ola, M.; Chawla, R.; Thakur, V.K. Hydrazone comprising compounds as promising anti-infective agents: Chemistry and structure-property relationship. *Mater. Today Chem.* **2020**, *18*, 100349. [CrossRef]
13. Koçak Aslan, E.; Krishna, V.S.; Armaković, S.J.; Armaković, S.; Şahin, O.; Tønjum, T.; Gündüz, M.G. Linking azoles to isoniazid via hydrazone bridge: Synthesis, crystal structure determination, antitubercular evaluation and computational studies. *J. Mol. Liq.* **2022**, *354*, 118873. [CrossRef]
14. Vavříková, E.; Polanc, S.; Kočevár, M.; Horváti, K.; Bószé, S.; Stolaříková, J.; Vávrová, K.; Vinšová, J. New fluorine-containing hydrazones active against MDR-tuberculosis. *Eur. J. Med. Chem.* **2011**, *46*, 4937–4945. [CrossRef] [PubMed]
15. Vergara, F.M.F.; Lima, C.H.d.S.; das Graças de Oliveira Henriques, M.; Candéa, A.L.P.; Lourenço, M.C.S.; de Lima Ferreira, M.; Kaiser, C.R.; de Souza, M.V.N. Synthesis and antimycobacterial activity of N'-(E)-(monosubstituted-benzylidene)-2-pyrazinecarbohydrazide derivatives. *Eur. J. Med. Chem.* **2009**, *44*, 4954–4959. [CrossRef] [PubMed]
16. Ivasiv, V.; Albertini, C.; Gonçalves, A.E.; Rossi, M.; Bolognesi, M.L. Molecular hybridization as a tool for designing multitarget drug candidates for complex diseases. *Curr. Top. Med. Chem.* **2019**, *19*, 1694–1711. [CrossRef] [PubMed]
17. Viegas, C., Jr.; Eliezer, J.B.; Manssour Fraga, C.A. Molecular Hybridization: A Useful Tool in the Design of New Drug Prototypes. *Curr. Med. Chem.* **2007**, *14*, 1829–1852. [CrossRef]
18. Stagg, H.R.; Lipman, M.C.; McHugh, T.D.; Jenkins, H.E. Isoniazid-resistant tuberculosis: A cause for concern? *Int. J. Tuberc. Lung Dis.* **2017**, *21*, 129–139. [CrossRef]
19. Tonge, P.; Kisker, C.; Slayden, R. Development of Modern InhA Inhibitors to Combat Drug Resistant Strains of Mycobacterium tuberculosis. *Curr. Top. Med. Chem.* **2007**, *7*, 489–498. [CrossRef]
20. Li, P.; Wang, B.; Fu, L.; Guo, K.; Ma, C.; Wang, B.; Lin, Z.; Li, G.; Huang, H.; Lu, Y. Identification of novel benzothioopyranones with ester and amide motifs derived from active metabolite as promising leads against Mycobacterium tuberculosis. *Eur. J. Med. Chem.* **2021**, *222*, 113603. [CrossRef]
21. Joaquim, A.R.; Gionbelli, M.P.; Gosmann, G.; Fuentesfria, A.M.; Lopes, M.S.; Fernandes De Andrade, S. Novel Antimicrobial 8-Hydroxyquinoline-Based Agents: Current Development, Structure-Activity Relationships, and Perspectives. *J. Med. Chem.* **2021**, *64*, 16349–16379. [CrossRef]
22. Lima, P.C.; Lima, L.M.; Da Silva, K.C.M.; Léda, P.H.O.; De Miranda, A.L.P.; Fraga, C.A.M.; Barreiro, E.J. Synthesis and analgesic activity of novel N-acylarylhydrazones and isosters, derived from natural safole. *Eur. J. Med. Chem.* **2000**, *35*, 187–203. [CrossRef]
23. Belowich, M.E.; Stoddart, J.F. Dynamic imine chemistry. *Chem. Soc. Rev.* **2012**, *41*, 2003–2024. [CrossRef] [PubMed]
24. Oliveira, P.F.M.; Guidetti, B.; Chamayou, A.; André-Barrès, C.; Madacki, J.; Korduláková, J.; Mori, G.; Orena, B.S.; Chiarelli, L.R.; Pasca, M.R.; et al. Mechanochemical Synthesis and Biological Evaluation of Novel Isoniazid Derivatives with Potent Antitubercular Activity. *Molecules* **2017**, *22*, 1457. [CrossRef] [PubMed]
25. Prasad, M.S.; Bhole, R.P.; Khedekar, P.B.; Chikhale, R.V. Mycobacterium enoyl acyl carrier protein reductase (InhA): A key target for antitubercular drug discovery. *Bioorg. Chem.* **2021**, *115*, 105242. [CrossRef]

26. Rivière, E.; Whitfield, M.G.; Nelen, J.; Heupink, T.H.; Van Rie, A. Identifying isoniazid resistance markers to guide inclusion of high-dose isoniazid in tuberculosis treatment regimens. *Clin. Microbiol. Infect.* **2020**, *26*, 1332–1337. [[CrossRef](#)] [[PubMed](#)]
27. Rožman, K.; Sosič, I.; Fernandez, R.; Young, R.J.; Mendoza, A.; Gobec, S.; Encinas, L. A new 'golden age' for the antitubercular target InhA. *Drug Discov. Today* **2017**, *22*, 492–502. [[CrossRef](#)]
28. Guardia, A.; Gulten, G.; Fernandez, R.; Gómez, J.; Wang, F.; Convery, M.; Blanco, D.; Martínez, M.; Pérez-Herrán, E.; Alonso, M.; et al. N-Benzyl-4-((heteroaryl)methyl)benzamides: A New Class of Direct NADH-Dependent 2-trans Enoyl-Acyl Carrier Protein Reductase (InhA) Inhibitors with Antitubercular Activity. *ChemMedChem* **2016**, *11*, 687–701. [[CrossRef](#)]
29. Chollet, A.; Maveyraud, L.; Lherbet, C.; Bernardes-Génisson, V. An overview on crystal structures of InhA protein: Apo-form, in complex with its natural ligands and inhibitors. *Eur. J. Med. Chem.* **2018**, *146*, 318–343. [[CrossRef](#)]
30. Lipinski, C.A.; Lombardo, F.; Dominy, B.W.; Feeney, P.J. Experimental and computational approaches to estimate solubility and permeability in drug discovery and development settings. *Adv. Drug Deliv. Rev.* **2001**, *46*, 3–26. [[CrossRef](#)]
31. Veber, D.F.; Johnson, S.R.; Cheng, H.Y.; Smith, B.R.; Ward, K.W.; Kopple, K.D. Molecular properties that influence the oral bioavailability of drug candidates. *J. Med. Chem.* **2002**, *45*, 2615–2623. [[CrossRef](#)]
32. Khan, S.R.; Manialawy, Y.; Siraki, A.G. Isoniazid and host immune system interactions: A proposal for a novel comprehensive mode of action. *Br. J. Pharmacol.* **2019**, *176*, 4599–4608. [[CrossRef](#)] [[PubMed](#)]
33. Kjellsson, M.C.; Via, L.E.; Goh, A.; Weiner, D.; Low, K.M.; Kern, S.; Pillai, G.; Barry, C.E.; Dartois, V. Pharmacokinetic evaluation of the penetration of antituberculosis agents in rabbit pulmonary lesions. *Antimicrob. Agents Chemother.* **2012**, *56*, 446–457. [[CrossRef](#)] [[PubMed](#)]
34. Ertl, P.; Rohde, B.; Selzer, P. Fast Calculation of Molecular Polar Surface Area as a Sum of Fragment-Based Contributions and Its Application to the Prediction of Drug Transport Properties. *J. Med. Chem.* **2000**, *43*, 3714–3717. [[CrossRef](#)] [[PubMed](#)]
35. Tokali, F.S.; Demir, Y.; Demircioğlu, İ.H.; Türkeş, C.; Kalay, E.; Şendil, K.; Beydemir, Ş. Synthesis, biological evaluation, and in silico study of novel library sulfonates containing quinazolin-4(3H)-one derivatives as potential aldose reductase inhibitors. *Drug Dev. Res.* **2022**, *83*, 586–604. [[CrossRef](#)] [[PubMed](#)]
36. Biava, M.; Porretta, G.C.; Poce, G.; Supino, S.; Deidda, D.; Pompei, R.; Mollicotti, P.; Manetti, F.; Botta, M. Antimycobacterial agents. Novel diarylpyrrole derivatives of BM212 endowed with high activity toward *Mycobacterium tuberculosis* and low cytotoxicity. *J. Med. Chem.* **2006**, *49*, 4946–4952. [[CrossRef](#)]
37. Atıcı, R.K.; Doğan, Ş.D.; Gündüz, M.G.; Krishna, V.S.; Chebaiki, M.; Homberset, H.; Lherbet, C.; Mourey, L.; Tønjum, T. Urea derivatives carrying a thiophenylthiazole moiety: Design, synthesis, and evaluation of antitubercular and InhA inhibitory activities. *Drug Dev. Res.* **2022**, *83*, 1292–1304. [[CrossRef](#)]
38. Rodriguez, F.; Saffon, N.; Sammartino, J.C.; Degiacomi, G.; Pasca, M.R.; Lherbet, C. First triclosan-based macrocyclic inhibitors of InhA enzyme. *Bioorg. Chem.* **2020**, *95*, 103498. [[CrossRef](#)]
39. Kuo, M.R.; Morbidoni, H.R.; Alland, D.; Sneddon, S.F.; Gourlie, B.B.; Staveski, M.M.; Leonard, M.; Gregory, J.S.; Janjigian, A.D.; Yee, C.; et al. Targeting Tuberculosis and Malaria through Inhibition of Enoyl Reductase. *J. Biol. Chem.* **2003**, *278*, 20851–20859. [[CrossRef](#)]
40. Wolber, G.; Langer, T. LigandScout: 3-D pharmacophores derived from protein-bound ligands and their use as virtual screening filters. *J. Chem. Inf. Model.* **2005**, *45*, 160–169. [[CrossRef](#)]
41. Morris, G.M.; Huey, R.; Lindstrom, W.; Sanner, M.F.; Belew, R.K.; Goodsell, D.S.; Olson, A.J. AutoDock4 and AutoDockTools4: Automated docking with selective receptor flexibility. *J. Comput. Chem.* **2009**, *30*, 2785–2791. [[CrossRef](#)]
42. *Schrödinger Release 2019-1: Maestro*; Schrödinger, LLC: New York, NY, USA, 2019.
43. Daina, A.; Michielin, O.; Zoete, V. SwissADME: A free web tool to evaluate pharmacokinetics, drug-likeness and medicinal chemistry friendliness of small molecules. *Sci. Rep.* **2017**, *7*, 42717. [[CrossRef](#)] [[PubMed](#)]